Proceedings Paper:
Liu, C., Yang, L. and Mihaylova, L.S. orcid.org/0000-0001-5856-2223 (2017) Dual-Satellite Source Geolocation with Time and Frequency Offsets and Satellite Location Errors. In: 2017 20th International Conference on Information Fusion (Fusion). 20th International Conference on Information Fusion, 10 - 13 July 2017, Xi'an, China. IEEE . ISBN 978-0-9964-5270-0

10.23919/ICIF.2017.8009716

Dual-Satellite Source Geolocation with Time and Frequency Offsets and Satellite Location Errors

Chao Liu[1], Le Yang[1,2], Lyudmila Mihaylova[1]

1 . Department of Automatic Control and Systems Engineering, University of Sheffield, Sheffield, S1 3JD, UK
2. School of Internet of Things (IoT) Engineering, Jiangnan University, Wuxi, 214122, China

{cliu47, le.yang, l.s.mihaylova}@sheffield.ac.uk

***Abstract*—This paper considers locating a static source on Earth using the time difference of arrival (TDOA) and frequency difference of arrival (FDOA) measurements obtained by a dual-satellite geolocation system. The TDOA and FDOA from the source are subject to unknown time and frequency offsets because the two satellites are imperfectly time-synchronized or frequency-locked. The satellite locations are not known accurately as well. To make the source position identifiable and mitigate the effect of satellite location errors, calibration stations at known positions are used. Achieving the maximum likelihood (ML) geolocation performance usually requires jointly estimating the source position and extra variables (i.e., time and frequency offsets as well as satellite locations), which is computationally intensive. In this paper, a novel closed-form geolocation algorithm is proposed. It first fuses the TDOA and FDOA measurements from the source and calibration stations to produce a single pair of TDOA and FDOA for source geolocation. This measurement fusion step eliminates the time and frequency offsets while taking into account the presence of satellite location errors. The source position is then found via standard TDOA-FDOA geolocation. The developed algorithm has low complexity and performance analysis shows that it attains the Cramér-Rao lower bound (CRLB) under Gaussian noises and mild conditions. Simulations using a challenging scenario with a short-baseline dual-satellite system verify the theoretical developments and demonstrate the good performance of the proposed algorithm.**

I. Introduction

Source geolocation refers to identifying the spatial position of a source on Earth using signal measurements such as the received signal strength (RSS), time of flight (TOF), time of arrival (TOA) and time difference of arrival (TDOA) [1], [2]. When the source is static, its position can be uniquely determined using a dual-satellite geolocation system with two satellites that are moving relatively to the source. First, the TDOA and frequency difference of arrival (FDOA) of the source signal received at the two satellites are estimated. The obtained TDOA and FDOA measurements are then exploited together with the source altitude information to achieve source geolocation using e.g., the algebraic algorithm in [3], or in reverse, determine the satellite orbits [4], [5]. Dual-satellite geolocation systems have found civilian and military applications including locating the ground interference to commercial satellites [6], [7] and space electronic reconnaissance [8].

The estimation of the source TDOA and FDOA requires joint processing of the source signals received at the two satellites for e.g., computing the cross ambiguity function (CAF) [9]–[11]. Therefore, precise time synchronization and frequency locking between the two satellites are needed for measuring TDOA and FDOA with high accuracy. However, in practice, time and frequency alignment could be difficult to attain. Consider the geolocation scenario shown in Fig. 1 for example, where satellite 1 transfers its received signal using a bent pipe transponder [12]. The TDOA and FDOA is estimated via cross-correlating the *downlink* signal from satellite 1 and the *uplink* signal from satellite 2. The obtained TDOA and FDOA may be subject to unknown time and frequency offsets, due to inaccurate knowledge on the group delay and local frequency of the satellite 1 transponder.

If the time and frequency offsets are small, they can be neglected in source geolocation and this would generally lead to biased source position estimates (see e.g., the analysis in [13]). When they have large absolute values, existing TDOA-FDOA geolocation algorithms such as those developed in [3], [8], [14] generally fail to produce a reasonable solution. This is because with only a pair of source TDOA and FDOA, it is not sufficient to geolocate the source while simultaneously estimating the time and frequency offsets. In other words, in the absence of time synchronization and frequency locking, the source position may become unidentifiable.

Precise knowledge on the satellite location information[1] is also essential for achieving satisfactory geolocation performance. It is well known that the presence of satellite location errors can significantly degrade the TDOA-FDOA geolocation

All authors contributed equally to this work.

Chao Liu and Lyudmila Mihaylova acknowledge the support from the UK Engineering and Physical Sciences Research Council (EPSRC) via the Bayesian Tracking and Reasoning over Time (BTaRoT) grant EP/K021516/1.

Le Yang acknowledges the support from the Chinese Scholarship Council (CSC).

[1]For simplicity, we use satellite location in this paper to represent satellite position and velocity.

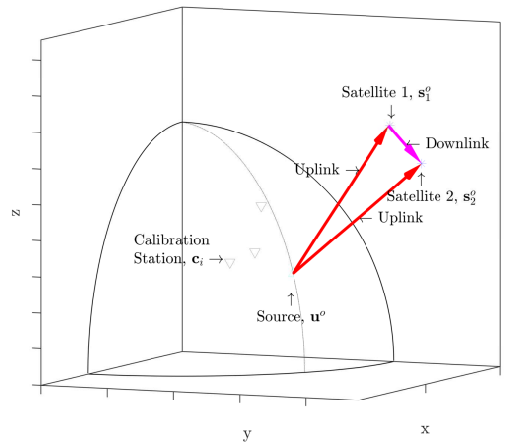

Fig. 1. Short-baseline dual-satellite geolocation scenario. Satellite 2 estimates the source and calibration TDOAs and FDOAs for source geolocation via cross-correlating the received downlink signal from satellite 1 and its own uplink signal.

accuracy [14]–[16]. However, the satellite location errors are almost inevitable because the satellites are moving and/or they are in orbits distant from Earth, making obtaining accurate satellite locations difficult.

In this paper, we investigate the use of calibration stations at known positions to improve the geolocation performance of the dual-satellite system when the two satellites have imperfect time and frequency alignment as well as erroneous locations. It is assumed that the source and calibration TDOAs and FDOAs are obtained within a short interval such that they are subject to the same time and frequency offsets and the same satellite location errors [17]–[19]. A new closed-form source geolocation algorithm is proposed for the above problem. In particular, it first fuses the measurements from the unknown source and calibration stations using a best linear unbiased estimator (BLUE) [20]. The time and frequency offsets are eliminated in the fusion process and the presence of satellite location errors is appropriately taken into account in the weighting matrix. The measurement fusion step only produces a single pair of source TDOA and FDOA, which is then utilized by an existing algebraic technique for source geolocation. The developed algorithm has low computational complexity, and more importantly, theoretical performance analysis shows that it can attain the Cramér-Rao lower bound (CRLB) under Gaussian noise and mild conditions. We illustrate the performance of the proposed algorithm via simulations based on the dual-satellite geolocation scenario shown in Fig. 1, which is challenging due to the short baseline between the two satellites. The obtained simulation results corroborate the theoretical developments.

Our work is different from [21] where precise sensor locations were assumed and source localization was achieved using a sequence of source TDOAs and FDOAs received during a short interval. A maximum likelihood (ML) estimator that jointly identifies the source position as well as time and frequency offsets was used in [21]. It is iterative and computationally intensive. In [13], [22]–[25], several techniques were proposed to deal with the problem of node localization in the presence of unknown clock offset in sensor networks. However, they all involved joint time synchronization and node localization based on iterative convex optimization [22] or closed-form methods [13], [23], [24]. Moreover, except for [24], they assumed accurate sensor locations.

Our work is more closely related to [26]–[29]. In [26], [27], the clock offset was removed by forming differential TDOAs (D-TDOAs) for node localization. They did not consider sensor position errors and an iterative ML location estimator was used. The algorithm developed in [28] eliminated the clock bias via the use of asymmetric trip ranging (ATR). This protocol required the node to be located to be cooperative, which may not be fulfilled in the dual-satellite geolocation problem considered in this paper. In [29], the sensors used for TDOA localization were partitioned into groups. Each group had a different clock offset, which was canceled out by taking differences between the TDOA measurements *within* each group. In contrast, the algorithm proposed in this paper eliminates the time and frequency offsets in *all* the measurements and fuses them using a BLUE to generate only a pair of source TDOA and FDOA for source geolocation.

The rest of this paper is organized as follows. We formulate the geolocation problem in consideration in Section II. The geolocation CRLB is derived in Section III. The proposed geolocation algorithm together with its performance analysis is presented in IV. Simulation results are given in Section V. Conclusions are drawn in Section VI.

II. Problem Formulation

We consider locating a static source on Earth whose unknown position is denoted by $\mathbf{u}^o = [u_x^o, u_y^o, u_z^o]^T$. Under the oblate spheroidal Earth model specified in World Geodetic System 1984 (WGS84), $\mathbf{u}^o$ is related to the source geodetic latitude ϕ and longitude φ via [30]

$$u_x^o = (r+h)\cos(\phi)\cos(\varphi) \tag{1a}$$
$$u_y^o = (r+h)\cos(\phi)\sin(\varphi) \tag{1b}$$
$$u_z^o = (r(1-e^2)+h)\sin(\phi) \tag{1c}$$

where $r = \frac{r_e}{\sqrt{1-e^2\sin^2\phi}}$, $r_e = 6378.137$ km is the equatorial radius, $e = 0.081819190842$ is the eccentricity, and h is the source altitude which is assumed to be known.

The dual-satellite system receives the source signal and computes the TDOA and FDOA between the two satellites. Let $\mathbf{s}_i^o = [s_{x,i}^o, s_{y,i}^o, s_{z,i}^o]^T$ and $\dot{\mathbf{s}}_i^o = [\dot{s}_{x,i}^o, \dot{s}_{y,i}^o, \dot{s}_{z,i}^o]^T$ be the true geocentric position and velocity of satellite i, $i = 1, 2$. Without time synchronization and frequency locking, the estimated source TDOA and FDOA can be expressed as [21], after being multiplied respectively with the signal propagation speed and the source signal wavelength,

$$y_u = d_u^o + \tau + \Delta y_u \tag{2a}$$
$$\dot{y}_u = \dot{d}_u^o + \delta + \Delta\dot{y}_u. \tag{2b}$$

τ and δ are the unknown time and frequency offsets between the two satellites. d_u^o and $\dot{d}_u^o$ are the true source TDOA and FDOA, and they are equal to

$$d_u^o = ||\mathbf{u}^o - \mathbf{s}_1^o|| - ||\mathbf{u}^o - \mathbf{s}_2^o|| \tag{3a}$$

$$\dot{d}_u^o = \frac{-(\mathbf{u}^o - \mathbf{s}_1^o)^T \dot{\mathbf{s}}_1^o}{||\mathbf{u}^o - \mathbf{s}_1^o||} - \frac{-(\mathbf{u}^o - \mathbf{s}_2^o)^T \dot{\mathbf{s}}_2^o}{||\mathbf{u}^o - \mathbf{s}_2^o||} \tag{3b}$$

where $||\cdot||$ represents the Euclidean distance. For notation simplicity, we collect y_u and $\dot{y}_u$ to form the source measurement vector $\mathbf{y}_u = [y_u, \dot{y}_u]^T$. Moreover, we introduce

$$\boldsymbol{\alpha}^o = [\tau, \delta]^T \tag{4}$$

to collect the time and frequency offsets. Note that with only $\mathbf{y}_u$, the source position is unidentifiable, due to the presence of the additional unknown $\boldsymbol{\alpha}^o$.

The true satellite location information is not available. The geolocation algorithm only has access to noisy observations of $\mathbf{s}_i^o$ and $\dot{\mathbf{s}}_i^o$, which are denoted as

$$\mathbf{s}_i = \mathbf{s}_i^o + \Delta\mathbf{s}_i \tag{5a}$$

$$\dot{\mathbf{s}}_i = \dot{\mathbf{s}}_i^o + \Delta\dot{\mathbf{s}}_i. \tag{5b}$$

Collecting the known satellite locations yields $\boldsymbol{\beta} = [\mathbf{s}_1^T, \dot{\mathbf{s}}_1^T, \mathbf{s}_2^T, \dot{\mathbf{s}}_2^T]^T$. Its true value is $\boldsymbol{\beta}^o = [\mathbf{s}_1^{oT}, \dot{\mathbf{s}}_1^{oT}, \mathbf{s}_2^{oT}, \dot{\mathbf{s}}_2^{oT}]^T$. The satellite location error vector is denoted by $\Delta\boldsymbol{\beta} = \boldsymbol{\beta} - \boldsymbol{\beta}^o = [\Delta\mathbf{s}_1^T, \Delta\dot{\mathbf{s}}_1^T, \Delta\mathbf{s}_2^T, \Delta\dot{\mathbf{s}}_2^T]^T$, which is assumed to be zero-mean Gaussian distributed with covariance matrix $\mathbf{Q}_\beta$ [14], [17]–[19], [24], [29].

There are N ground calibration stations at known positions $\mathbf{c}_n = [c_{x,n}, c_{y,n}, c_{z,n}]^T$, $n = 1, 2, ..., N$, deployed to improve the geolocation accuracy in the absence of time and frequency alignment between satellites and precise satellite locations. When the measurements from the unknown source and calibration stations are obtained during a short interval, they would be subject to the same time and frequency offsets. As a result, the calibration TDOAs and FDOAs can be modeled similar to (2) as

$$y_{c,n} = d_{c,n}^o + \tau + \Delta y_{c,n} \tag{6a}$$

$$\dot{y}_{c,n} = \dot{d}_{c,n}^o + \delta + \Delta\dot{y}_{c,n}. \tag{6b}$$

$d_{c,n}^o$ and $\dot{d}_{c,n}^o$ are the true TDOA and FDOA from the n-th calibration station, which are equal to

$$d_{c,n}^o = ||\mathbf{c}_n - \mathbf{s}_1^o|| - ||\mathbf{c}_n - \mathbf{s}_2^o|| \tag{7a}$$

$$\dot{d}_{c,n}^o = \frac{-(\mathbf{c}_n - \mathbf{s}_1^o)^T \dot{\mathbf{s}}_1^o}{||\mathbf{c}_n - \mathbf{s}_1^o||} - \frac{-(\mathbf{c}_n - \mathbf{s}_2^o)^T \dot{\mathbf{s}}_2^o}{||\mathbf{c}_n - \mathbf{s}_2^o||}. \tag{7b}$$

It can be seen from (6) that with calibration stations, the source position becomes identifiable because there are $(N+1) \geq 2$ pairs of measurements, which are sufficient to determine the source position and time and frequency offsets.

Collecting $y_{c,n}$ and $\dot{y}_{c,n}$, and stacking the results over n yield the calibration measurement vector $\mathbf{y}_c = [\mathbf{y}_{c,1}^T, \mathbf{y}_{c,2}^T, ..., \mathbf{y}_{c,N}^T]^T$, where $\mathbf{y}_{c,n} = [y_{c,n}, \dot{y}_{c,n}]^T$. Combining the source measurement vector $\mathbf{y}_u$ with $\mathbf{y}_c$ yields the composite measurement vector $\mathbf{y} = [\mathbf{y}_u^T, \mathbf{y}_c^T]^T$. According to (2) and (6), the true value of $\mathbf{y}$ can be expressed as

$$\mathbf{y}^o = [\mathbf{d}_u^{oT}, \mathbf{d}_{c,1}^{oT}, \mathbf{d}_{c,2}^{oT}, ..., \mathbf{d}_{c,N}^{oT}]^T + \mathbf{G}\boldsymbol{\alpha}^o. \tag{8}$$

The coefficient matrix $\mathbf{G}$ is equal to

$$\mathbf{G} = \mathbf{1}_{(N+1)\times 1} \otimes \mathbf{I}_{2\times 2} \tag{9}$$

where $\otimes$ denotes the Kronecker product, $\mathbf{1}_{(N+1)\times 1}$ denotes a $(N+1)\times 1$ column vector of ones and $\mathbf{I}_{2\times 2}$ represents a 2×2 identity matrix. The vectors $\mathbf{d}_u^o$ and $\mathbf{d}_{c,n}^o$ are defined as

$$\mathbf{d}_u^o = [d_u^o, \dot{d}_u^o]^T \tag{10a}$$

$$\mathbf{d}_{c,n}^o = [d_{c,n}^o, \dot{d}_{c,n}^o]^T. \tag{10b}$$

The measurement noise in $\mathbf{y}$ can be shown to be $\Delta\mathbf{y} = \mathbf{y} - \mathbf{y}^o = [\Delta y_u, \Delta\dot{y}_u, \Delta y_{c,1}, \Delta\dot{y}_{c,1}, ..., \Delta y_{c,N}, \Delta\dot{y}_{c,N}]^T$. As in [17]–[19], it is assumed that $\Delta\mathbf{y}$ is a zero-mean Gaussian random vector with covariance matrix $\mathbf{Q}_y$ and $\Delta\mathbf{y}$ is also independent of the satellite location error $\Delta\boldsymbol{\beta}$.

We are interested in estimating at a low computational cost the source position $\mathbf{u}^o$ using the source and calibration TDOAs and FDOAs in $\mathbf{y}$ as well as the noisy satellite locations in $\boldsymbol{\beta}$.

III. CRLB

This section derives the CRLB of $\mathbf{u}^o$, denoted by CRLB($\mathbf{u}^o$). For this purpose, note that according to the previous section, besides the source position $\mathbf{u}^o$, the time and frequency offsets in $\boldsymbol{\alpha}^o$ and true satellite location vector $\boldsymbol{\beta}^o$ are also unknown. As the source altitude h is known, the CRLB of $[\mathbf{u}^{oT}, \boldsymbol{\alpha}^{oT}, \boldsymbol{\beta}^{oT}]^T$ would be an equality-constrained one [31]. To simplify the derivation, we follow the re-parameterization approach [32] and establish CRLB($\mathbf{u}^o$) via relating it to the CRLB of $\boldsymbol{\theta}^o = [\phi, \varphi]^T$, where ϕ and φ are the source geodetic latitude and longitude (see (1)). Specifically, we have [20]

$$\text{CRLB}(\mathbf{u}^o) = \left(\frac{\partial \mathbf{u}^o}{\partial \boldsymbol{\theta}^o}\right) \cdot \text{CRLB}(\boldsymbol{\theta}^o) \cdot \left(\frac{\partial \mathbf{u}^o}{\partial \boldsymbol{\theta}^o}\right)^T. \tag{11}$$

To find CRLB($\boldsymbol{\theta}^o$), we need to derive the CRLB of the composite unknown vector $\boldsymbol{\eta}^o = [\boldsymbol{\theta}^{oT}, \boldsymbol{\alpha}^{oT}, \boldsymbol{\beta}^{oT}]^T$ first. Express $\boldsymbol{\eta}^o$ as $\boldsymbol{\eta}^o = [\boldsymbol{\gamma}^{oT}, \boldsymbol{\beta}^{oT}]^T$, where $\boldsymbol{\gamma}^o = [\boldsymbol{\theta}^{oT}, \boldsymbol{\alpha}^{oT}]^T$ contains the source position as well as time and frequency offsets.

Note from Section II that the composite TDOA and FDOA measurement vector $\mathbf{y}$ and the known satellite locations $\boldsymbol{\beta}$ are jointly Gaussian distributed. Taking logarithm of this joint distribution, differentiating it twice with respect to $\boldsymbol{\eta}^o$, negating the sign and taking expectation yields the Fisher information matrix (FIM) of $\boldsymbol{\eta}^o$ [20]. The partitioned matrix form of FIM($\boldsymbol{\eta}^o$) is

$$\text{FIM}(\boldsymbol{\eta}^o) = \begin{bmatrix} \mathbf{X} & \mathbf{Y} \\ \mathbf{Y}^T & \mathbf{Z} \end{bmatrix}. \tag{12}$$

The matrix partitions are defined as

$$\mathbf{X} = \left(\frac{\partial \mathbf{y}^o}{\partial \boldsymbol{\gamma}^o}\right)^T \mathbf{Q}_y^{-1} \left(\frac{\partial \mathbf{y}^o}{\partial \boldsymbol{\gamma}^o}\right) \tag{13a}$$

$$\mathbf{Y} = \left(\frac{\partial \mathbf{y}^o}{\partial \boldsymbol{\gamma}^o}\right)^T \mathbf{Q}_y^{-1} \left(\frac{\partial \mathbf{y}^o}{\partial \boldsymbol{\beta}^o}\right) \tag{13b}$$

$$\mathbf{Z} = \mathbf{Q}_\beta^{-1} + \left(\frac{\partial \mathbf{y}^o}{\partial \boldsymbol{\beta}^o}\right)^T \mathbf{Q}_y^{-1} \left(\frac{\partial \mathbf{y}^o}{\partial \boldsymbol{\beta}^o}\right). \tag{13c}$$

$\mathbf{X}$ is the FIM of $\boldsymbol{\gamma}^o$ when the satellite location errors are absent. Inversing FIM($\boldsymbol{\eta}^o$) gives CRLB($\boldsymbol{\eta}^o$), and its upper-left 2×2 block is the desired CRLB($\boldsymbol{\theta}^o$).

We shall derive a detailed expression for CRLB($\boldsymbol{\theta}^o$) to gain insights. First, taking the inverse of FIM($\boldsymbol{\eta}^o$) and retaining only the upper-left 4×4 block yield the CRLB of $\boldsymbol{\gamma}^o$, which is given by

$$\text{CRLB}(\boldsymbol{\gamma}^o) = \left(\mathbf{X} - \mathbf{Y}\mathbf{Z}^{-1}\mathbf{Y}^T\right)^{-1}. \tag{14}$$

Putting the definitions of $\mathbf{X}$, $\mathbf{Y}$ and $\mathbf{Z}$ and applying the matrix inversion Lemma [20], we arrive at

$$\text{CRLB}(\boldsymbol{\gamma}^o) = \left(\left(\frac{\partial \mathbf{y}^o}{\partial \boldsymbol{\gamma}^o}\right)^T \tilde{\mathbf{Q}}_y^{-1} \left(\frac{\partial \mathbf{y}^o}{\partial \boldsymbol{\gamma}^o}\right)\right)^{-1} \tag{15}$$

where

$$\tilde{\mathbf{Q}}_y = \mathbf{Q}_y + \left(\frac{\partial \mathbf{y}^o}{\partial \boldsymbol{\beta}^o}\right) \mathbf{Q}_\beta \left(\frac{\partial \mathbf{y}^o}{\partial \boldsymbol{\beta}^o}\right)^T. \tag{16}$$

It is easy to show that $\tilde{\mathbf{Q}}_y - \mathbf{Q}_y$ is positive semi-definite. Moreover, $\tilde{\mathbf{Q}}_y$ is generally not block diagonal, even if the TDOA and FDOA measurements from the source and calibration stations are independent to one another and $\mathbf{Q}_y$ has a block diagonal structure. As a result, by taking the inverse of CRLB($\boldsymbol{\gamma}^o$) in (15) and comparing the result with (13a), we have that FIM($\boldsymbol{\gamma}^o$) = CRLB($\boldsymbol{\gamma}^o$)$^{-1}$ can be considered as the FIM of $\boldsymbol{\gamma}^o$ when accurate satellite locations are known but the measurements have an *increased* covariance matrix $\tilde{\mathbf{Q}}_y$. In other words, satellite location errors affect the estimation of the source position and time and frequency offsets via degrading and introducing *extra* correlation into the source and calibration measurements.

According to the definition $\boldsymbol{\gamma}^o = [\boldsymbol{\theta}^{oT}, \boldsymbol{\alpha}^{oT}]^T$, CRLB($\boldsymbol{\theta}^o$) is given by the upper-left 2×2 block of CRLB($\boldsymbol{\gamma}^o$). To evaluate (15), we put (8) and express the partial derivative $(\frac{\partial \mathbf{y}^o}{\partial \boldsymbol{\gamma}^o})$ as

$$\left(\frac{\partial \mathbf{y}^o}{\partial \boldsymbol{\gamma}^o}\right) = \left[\mathbf{H}\left(\frac{\partial \mathbf{d}_u^o}{\partial \boldsymbol{\theta}^o}\right), \mathbf{G}\right] \tag{17}$$

where $\mathbf{G}$ is defined in (9), the matrix $\mathbf{H}$ is defined as

$$\mathbf{H} = \begin{bmatrix} \mathbf{I}_{2\times2} \\ \mathbf{O}_{N\times2} \end{bmatrix} \tag{18}$$

and N is the number of calibration stations. Substituting (17) into (15) and applying the partitioned matrix inversion formula [20] yield

$$\text{CRLB}(\boldsymbol{\theta}^o) = \left(\left(\frac{\partial \mathbf{d}_u^o}{\partial \boldsymbol{\theta}^o}\right)^T \left(\mathbf{H}^T \mathbf{P}_y \mathbf{H}\right) \left(\frac{\partial \mathbf{d}_u^o}{\partial \boldsymbol{\theta}^o}\right)\right)^{-1}. \tag{19}$$

which is the desired form for CRLB($\boldsymbol{\theta}^o$). The matrix $\mathbf{P}_y$ is equal to

$$\mathbf{P}_y = \tilde{\mathbf{Q}}_y^{-1} - \tilde{\mathbf{Q}}_y^{-1}\mathbf{G}\left(\mathbf{G}^T\tilde{\mathbf{Q}}_y^{-1}\mathbf{G}\right)^{-1}\mathbf{G}^T\tilde{\mathbf{Q}}_y^{-1}. \tag{20}$$

$\mathbf{P}_y$ is in fact a singular matrix, which can be verified as follows. Applying the Cholesky decomposition $\tilde{\mathbf{Q}}_y = \tilde{\mathbf{L}}_y\tilde{\mathbf{L}}_y^T$ to (20), we obtain $\mathbf{P}_y = \tilde{\mathbf{L}}_y^{-T}\mathbf{P}\tilde{\mathbf{L}}_y^{-1}$, where

$$\mathbf{P} = \mathbf{I}_{(N+1)\times2} - \tilde{\mathbf{L}}_y^{-1}\mathbf{G}\left(\mathbf{G}^T\tilde{\mathbf{L}}_y^{-T}\tilde{\mathbf{L}}_y^{-1}\mathbf{G}\right)^{-1}\mathbf{G}^T\tilde{\mathbf{L}}_y^{-T}. \tag{21}$$

$\mathbf{P}$ is clearly a projection matrix, which is singular and renders $\mathbf{P}_y$ non-invertible.

Note that the three terms on the right-hand side of (19) are all 2×2 matrices. For CRLB($\boldsymbol{\theta}^o$) to be existent, they must be non-singular. Hence, substituting (19) back to (11) gives

$$\begin{aligned}&\text{CRLB}(\mathbf{u}^o) \\ &= \left(\frac{\partial \mathbf{u}^o}{\partial \boldsymbol{\theta}^o}\right)\left(\frac{\partial \mathbf{d}_u^o}{\partial \boldsymbol{\theta}^o}\right)^{-1}\left(\mathbf{H}^T\mathbf{P}_y\mathbf{H}\right)^{-1}\left(\frac{\partial \mathbf{d}_u^o}{\partial \boldsymbol{\theta}^o}\right)^{-T}\left(\frac{\partial \mathbf{u}^o}{\partial \boldsymbol{\theta}^o}\right)^T.\end{aligned} \tag{22}$$

This is the CRLB of the source position $\mathbf{u}^o$ under the considered dual-satellite geolocation scenario where unknown time and frequency offsets between satellites and satellite location errors are present. It lower-bounds the error covariance matrix of any unbiased estimator of $\mathbf{u}^o$. The required partial derivatives, $\left(\frac{\partial \mathbf{u}^o}{\partial \boldsymbol{\theta}^o}\right)$, $\left(\frac{\partial \mathbf{d}_u^o}{\partial \boldsymbol{\theta}^o}\right)$ and $\left(\frac{\partial \mathbf{y}^o}{\partial \boldsymbol{\beta}^o}\right)$, are given in the Appendix.

Carefully examining (22) reveals that the source position CRLB does not depend on the actual values of the time and frequency offsets. More importantly, it has the same functional form as the geolocation CRLB with precise time-frequency alignment between satellites, accurate satellite locations and a source TDOA-FDOA covariance matrix $(\mathbf{H}^T\mathbf{P}_y\mathbf{H})^{-1}$ (see e.g., [3]). The measurements from calibration stations affects the source geolocation performance only through the term $(\mathbf{H}^T\mathbf{P}_y\mathbf{H})^{-1}$. These observations are essential for the low-complexity geolocation algorithm development in the following section.

IV. Algorithm

The geolocation algorithm development begins with noting from (6) and (7) that the TDOA and FDOA measurements from calibration stations are not dependent on the source position $\mathbf{u}^o$. According to the CRLB analysis in Section III, they contribute to the source geolocation accuracy *indirectly* through providing information on the time and frequency offsets $\boldsymbol{\alpha}^o$ and true satellite locations.

In this paper, we shall develop a novel two-step algorithm that avoids the estimation of *any* extra variables (i.e., the true satellite locations $\boldsymbol{\beta}^o$ as well as the time and frequency offsets $\boldsymbol{\alpha}^o$). Step-1 of the proposed algorithm fuses the TDOA and FDOA measurements from the unknown source and calibration stations using a BLUE. It eliminates $\boldsymbol{\alpha}^o$ and takes into account the presence of satellite location errors in the weighting matrix. The output of Step-1, which is an estimate

of the source TDOA and FDOA d_u^o and $\dot{d}_u^o$ (see (3)), is utilized in Step-2 of the proposed algorithm for geolocating the source.

Step-1: We start with considering the composite measurement vector $\mathbf{y} = \mathbf{y}^o + \Delta\mathbf{y}$ that contains the TDOAs and FDOAs from the source and calibration stations. Note from (3) and (7) that the true value of $\mathbf{y}$, $\mathbf{y}^o$, depends on the true satellite locations $\boldsymbol{\beta}^o$, which is unknown. We therefore approximate $\mathbf{y}^o$, after applying the first-order Taylor-Series expansion around the known satellite locations $\boldsymbol{\beta}$, as

$$\mathbf{y}^o \approx \hat{\mathbf{y}}^o - \mathbf{D}\Delta\boldsymbol{\beta} \tag{23}$$

where

$$\hat{\mathbf{y}}^o = \left[\hat{\mathbf{d}}_u^{oT}, \hat{\mathbf{d}}_{c,1}^T, ..., \hat{\mathbf{d}}_{c,N}^T\right]^T + \mathbf{G}\boldsymbol{\alpha}^o. \tag{24}$$

$\hat{\mathbf{d}}_u^o = [\hat{d}_u^o, \hat{\dot{d}}_u^o]^T$ and $\hat{\mathbf{d}}_{c,n} = [\hat{d}_{c,n}.\hat{\dot{d}}_{c,n}]^T$ have the same functional forms as $\mathbf{d}_u^o$ in (3) and $\mathbf{d}_{c,n}^o$ in (7) except that the true satellite locations $\boldsymbol{\beta}^o$ are replaced with their known but noisy version $\boldsymbol{\beta}$. Mathematically, we have

$$\hat{d}_u^o = ||\mathbf{u}^o - \mathbf{s}_1|| - ||\mathbf{u}^o - \mathbf{s}_2|| \tag{25a}$$

$$\hat{\dot{d}}_u^o = \frac{-(\mathbf{u}^o - \mathbf{s}_1)^T\dot{\mathbf{s}}_1}{||\mathbf{u}^o - \mathbf{s}_1||} - \frac{-(\mathbf{u}^o - \mathbf{s}_2)^T\dot{\mathbf{s}}_2}{||\mathbf{u}^o - \mathbf{s}_2||} \tag{25b}$$

$$\hat{d}_{c,n} = ||\mathbf{c}_n - \mathbf{s}_1|| - ||\mathbf{c}_n - \mathbf{s}_2|| \tag{25c}$$

$$\hat{\dot{d}}_{c.n} = \frac{-(\mathbf{c}_n - \mathbf{s}_1)^T\dot{\mathbf{s}}_1}{||\mathbf{c}_n - \mathbf{s}_1||} - \frac{-(\mathbf{c}_n - \mathbf{s}_2)^T\dot{\mathbf{s}}_2}{||\mathbf{c}_n - \mathbf{s}_2||} \tag{25d}$$

where $n = 1, 2, ..., N$. The coefficient matrix $\mathbf{D}$ for the satellite location error $\Delta\boldsymbol{\beta}$ can be shown to be

$$\mathbf{D} = \left(\frac{\partial\hat{\mathbf{y}}^o}{\partial\boldsymbol{\beta}}\right). \tag{26}$$

Putting (24) and (25) into (26) and comparing the result with (40) indicate that $\mathbf{D}$ is equal to the partial derivative $\left(\frac{\partial\mathbf{y}^o}{\partial\boldsymbol{\beta}^o}\right)$ evaluated at the noisy satellite locations $\boldsymbol{\beta}$.

Note from (25) that $\dot{\mathbf{d}}_{c,n}$ are indeed a known quantity because the calibration station positions $\mathbf{c}_n$ and satellite locations $\boldsymbol{\beta}$ are both available. Exploring the above fact and putting (24) transform the composite measurement vector $\mathbf{y}$ into

$$\hat{\mathbf{y}} \approx \mathbf{H}\hat{\mathbf{d}}_u^o + \mathbf{G}\boldsymbol{\alpha}^o + (\Delta\mathbf{y} - \mathbf{D}\Delta\boldsymbol{\beta}) \tag{27}$$

where $\mathbf{G}$ and $\mathbf{H}$ are defined in (9) and (18). Besides,

$$\hat{\mathbf{y}} = \mathbf{y} - [\mathbf{0}^T, \hat{\mathbf{d}}_{c,1}^T, ..., \hat{\mathbf{d}}_{c,N}^T]^T. \tag{28}$$

We shall estimate the source TDOA and FDOA $\hat{\mathbf{d}}_u^o$ from $\hat{\mathbf{y}}$ to accomplish the desired measurement fusion. For this purpose, note that in (27), the noise term $(\Delta\mathbf{y} - \mathbf{D}\Delta\boldsymbol{\beta})$ is zero-mean Gaussian distributed with covariance matrix

$$\hat{\mathbf{Q}}_y = \mathbf{Q}_y + \mathbf{D}\mathbf{Q}_\beta\mathbf{D}^T \tag{29}$$

because $\Delta\mathbf{y}$ and $\Delta\boldsymbol{\beta}$ are independent zero-mean Gaussian random vectors with covariance matrices $\mathbf{Q}_y$ and $\mathbf{Q}_\beta$ (see Section II). We eliminate the time and frequency offsets $\boldsymbol{\alpha}^o$ in (27) by first pre-whitening the noise in $\hat{\mathbf{y}}$ using $\hat{\mathbf{L}}_y^{-1}$ and then multiplying both sides of (27) by the projection matrix

$$\hat{\mathbf{P}} = \mathbf{I}_{(N+1)\times 2} - \hat{\mathbf{L}}_y^{-1}\mathbf{G}\left(\mathbf{G}^T\hat{\mathbf{L}}_y^{-T}\hat{\mathbf{L}}_y^{-1}\mathbf{G}\right)^{-1}\mathbf{G}^T\hat{\mathbf{L}}_y^{-T}. \tag{30}$$

Here, $\hat{\mathbf{Q}}_y = \hat{\mathbf{L}}_y\hat{\mathbf{L}}_y^T$ is the Cholesky decomposition of $\hat{\mathbf{Q}}_y$. After these manipulations, (27) becomes

$$\hat{\mathbf{P}}\hat{\mathbf{L}}_y^{-1}\hat{\mathbf{y}} = \hat{\mathbf{P}}\hat{\mathbf{L}}_y^{-1}\mathbf{H}\hat{\mathbf{d}}_u^o + \hat{\mathbf{P}}\hat{\mathbf{L}}_y^{-1}(\Delta\mathbf{y} - \mathbf{D}\Delta\boldsymbol{\beta}) \tag{31}$$

where $\hat{\mathbf{P}}\mathbf{G} = 0$ has been applied. The BLUE of $\hat{\mathbf{d}}_u^o$ is [20], [33]

$$\hat{\mathbf{d}}_u = [\hat{d}_u, \hat{\dot{d}}_u]^T = \left(\mathbf{H}^T\hat{\mathbf{P}}_y\mathbf{H}\right)^{-1}\mathbf{H}^T\hat{\mathbf{P}}_y\hat{\mathbf{y}} \tag{32}$$

where the fact that $\hat{\mathbf{Q}}_y^{-1} = \hat{\mathbf{L}}_y^{-T}\hat{\mathbf{L}}_y^{-1}$ and $\hat{\mathbf{P}}$ is idempotent (i.e., $\hat{\mathbf{P}}^2 = \hat{\mathbf{P}}$) has been applied, and

$$\hat{\mathbf{P}}_y = \hat{\mathbf{Q}}_y^{-1} - \hat{\mathbf{Q}}_y^{-1}\mathbf{G}\left(\mathbf{G}^T\hat{\mathbf{Q}}_y^{-1}\mathbf{G}\right)^{-1}\mathbf{G}^T\hat{\mathbf{Q}}_y^{-1}. \tag{33}$$

This completes the Step-1 processing of the proposed algorithm that fuses the source and calibration measurements.

It is worthwhile to point out that the approach used to cancel $\boldsymbol{\alpha}^o$ in (27) is referred to as orthogonal subspace projection (OSP) in some literature [33]–[35]. Recent study [33] showed that results identical to the fusion output in (32) can be obtained via jointly estimating $\hat{\mathbf{d}}_u^o$ and $\boldsymbol{\alpha}^o$, or "differential signal processing", where measurement differencing is used to eliminate $\boldsymbol{\alpha}^o$. In this work, we adopt the OSP approach to facilitate the performance analysis of the proposed algorithm.

Step-2: With the source TDOA and FDOA estimates in (32), the source position $\mathbf{u}^o$ can be estimated using e.g., the algebraic TDOA-FDOA geolocation technique developed in [3][2] that jointly utilizes $\hat{d}_u$, $\hat{\dot{d}}_u$, the source altitude h and known satellite locations $\boldsymbol{\beta}$. The obtained source position estimate, denoted by $\mathbf{u}$, is the algorithm output.

A. Implementation Aspect

Realizing the proposed algorithm requires the evaluation of $\hat{\mathbf{Q}}_y$ defined in (29). However, it depends on the unknown source position $\mathbf{u}^o$ through the matrix $\mathbf{D}$ define in (26). To address this difficulty, we set $\hat{\mathbf{Q}}_y = \mathbf{Q}_y$ to obtain an initial estimate of $\mathbf{u}^o$ and then plug the result back to (26) and (29) so that improved estimates of $\hat{\mathbf{Q}}_y$ and $\mathbf{u}^o$ can be obtained. In the algorithm implementation, we do not iterate the above process and simulations show that this approximation does not lead to observable performance degradation.

B. Performance Analysis

We derive the covariance matrix of the source position estimate $\mathbf{u}$, denoted by $\text{cov}(\mathbf{u})$, and compare it with $\text{CRLB}(\mathbf{u}^o)$. Note that the proposed algorithm finds $\mathbf{u}$ from $\hat{\mathbf{d}}_u$ in (32), which is the estimate of the source TDOA and FDOA $\hat{\mathbf{d}}_u^o = [\hat{d}_u^o, \hat{\dot{d}}_u^o]^T$ (see (25)). Following the same approach adopted in [3], we can show that $\text{cov}(\mathbf{u})$ is approximately equal to

$$\text{cov}(\mathbf{u}) \approx \left(\frac{\partial\mathbf{u}^o}{\partial\boldsymbol{\theta}^o}\right)\left(\frac{\partial\hat{\mathbf{d}}_u^o}{\partial\boldsymbol{\theta}^o}\right)^{-1}\text{cov}(\hat{\mathbf{d}}_u)\left(\frac{\partial\hat{\mathbf{d}}_u^o}{\partial\boldsymbol{\theta}^o}\right)^{-T}\left(\frac{\partial\mathbf{u}^o}{\partial\boldsymbol{\theta}^o}\right)^T \tag{34}$$

[2]This algorithm was indeed used to generate the simulation results presented in Section V.

where $\text{cov}(\hat{\mathbf{d}}_u)$ is the covariance matrix of $\hat{\mathbf{d}}_u$. It can be derived by putting (27) into (32) and subtracting $\hat{\mathbf{d}}_u^o$ from both sides to obtain the estimation error in $\hat{\mathbf{d}}_u$. Post-multiplying the estimation error with its transpose and taking expectation yield

$$\text{cov}(\hat{\mathbf{d}}_u) = \left(\mathbf{H}^T \hat{\mathbf{P}}_y \mathbf{H}\right)^{-1}. \tag{35}$$

Putting (35) and comparing (34) with (22) indicate that

$$\text{cov}(\mathbf{u}) \approx \text{CRLB}(\mathbf{u}^o) \tag{36}$$

if $\left(\frac{\partial \dot{\mathbf{d}}_u^o}{\partial \boldsymbol{\theta}^o}\right) \approx \left(\frac{\partial \mathbf{d}_u^o}{\partial \boldsymbol{\theta}^o}\right)$ and $\mathbf{P}_y \approx \hat{\mathbf{P}}_y$ (i.e., $\tilde{\mathbf{Q}}_y \approx \hat{\mathbf{Q}}_y$ or equivalently $\mathbf{D} \approx \left(\frac{\partial \mathbf{y}^o}{\partial \boldsymbol{\beta}}\right)$). It can be verified that the above approximations are valid under the conditions $\Delta \mathbf{s}_i / ||\mathbf{u}^o - \mathbf{s}_i^o|| \approx 0$ and $\Delta \dot{\mathbf{s}}_i / ||\mathbf{u}^o - \mathbf{s}_i^o|| \approx 0$ for $i = 1, 2$. In other words, when the satellite location errors are negligible with respect to the source-satellite range, the proposed algorithm can attain the CRLB accuracy under Gaussian noise model.

The above analysis implicitly assumes that the matrix $\mathbf{D}$ is evaluated using the *true* source position. Similar assumption was also utilized in [17]–[19], [24], [29]. However, as pointed out in the previous subsection, the algorithm implementation uses the *estimated* source position instead to produce $\mathbf{D}$. The amount of error introduced is dependent on the TDOA and FDOA noise as well as satellite location errors. As a result, the estimation performance of the proposed technique would eventually deviate from CRLB when the noise level becomes sufficiently large and the thresholding effect [20] occurs.

V. Simulations

We study the performance of the proposed two-step source geolocation algorithm via simulations. The performance metrics used are the geolocation root mean square error (RMSE), $\text{RMSE}(\mathbf{u}) = \sqrt{\frac{1}{K}\sum_{k=1}^{K} \|\mathbf{u}_k - \mathbf{u}^o\|^2}$, and the estimation bias, $\text{Bias}(\mathbf{u}) = \|\frac{1}{K}\sum_{k=1}^{K} \mathbf{u}_k - \mathbf{u}^o\|$. Here, $K = 20000$ is the number of Monte Carlo runs and $\mathbf{u}_k$ denotes the geolocation result in the k-th ensemble run.

The geolocation performance of the proposed algorithm is compared with the CRLB and that of two benchmark methods, namely an iterative ML estimator and a differential calibration (DC)-based estimator [15], [17]. The maximum likelihood (ML) algorithm estimates the source latitude and longitude $\boldsymbol{\theta}^o$ together with the time and frequency offsets $\boldsymbol{\alpha}^o$ and true satellite locations $\boldsymbol{\beta}^o$. The estimate of the geocentric position of the source is then found by plugging the result into (1). We initialize the ML algorithm via adding to the true values zero-mean Gaussian noise with covariance matrix equal to $4 \cdot \text{FIM}(\boldsymbol{\eta}^o)^{-1}$, where $\text{FIM}(\boldsymbol{\eta}^o)$ is given in (12). The DC-based method cancels $\boldsymbol{\alpha}^o$ by subtracting from the calibration measurements the source TDOA and FDOA and performing source geolocation using the transformed calibration measurements. Note that the satellite location errors are not explicitly taken into account in the DC-based method.

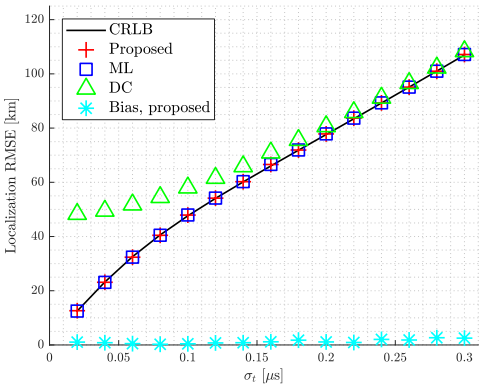

Fig. 2. Geolocation RMSE as a function of the TDOA noise standard deviation σ_t.

A. Setup

The simulated dual-satellite geolocation scenario is depicted in Fig. 1. The source is located at [124^{o}E, 25^{o}N] with known altitude $h = 100$m. There are three ground calibration stations and they are located at [116.3^{o}E, 39.9^{o}N], [119^{o}E, 39^{o}N] and [121^{o}E, 31.5^{o}N]. Two satellites are located at [86.71^{o}E, 0.029^{o}S] and [86.78^{o}E, 0.042^{o}S] with altitudes 35792km and 35742km. They are moving with velocities $\dot{\mathbf{s}}_1^o = [3.76, -0.67, 126.5]^T$m/s and $\dot{\mathbf{s}}_2^o = [1.27, 0.15, 133.7]^T$m/s. This simulation scenario is challenging mainly because the baseline (i.e., the distance between two satellites) is around 72km, which is much smaller than the source-satellite distance of more than 37778km. Hence, is a short-baseline geolocation geometry.

The source carrier frequency is $f_c = 14.5$GHz. To simplify the simulation, the carrier frequencies of the calibration stations are all set to be f_c as well, although in practice, they could be different from but close to f_c. The transponder at satellite 1 is assumed to have a group delay of 0.06μs and a local oscillator of 2.5GHz, both of which are unknown. We set that the covariance matrix for the source and calibration measurements $\mathbf{Q}_y$ is a diagonal matrix. Unless stated otherwise, the standard deviations of the TDOA and FDOA noises are σ_t = 0.1μs and σ_f = 10mHz, while the standard deviations of the satellite position and velocity errors are $\sigma_s = 1000$m and $\sigma_{\dot{s}} = 0.01$m/s.

B. Results

Fig. 2 plots as a function of the TDOA noise standard deviation σ_t the geolocation RMSE of the proposed two-step algorithm. It can be seen that the two-step method can provide geolocation accuracy very close to the CRLB when $\sigma_t \leq 0.25\mu$s, which is consistent with the performance analysis in Section III.B. The ML estimator is also able to attain the CRLB accuracy but at the cost of higher computational complexity due to iteratively estimating the source position and extra variables in a joint manner. In terms of running time, the proposed algorithm is at least 2 times faster than the ML method on our desktop with Intel Core i5-4590 3.30GHz

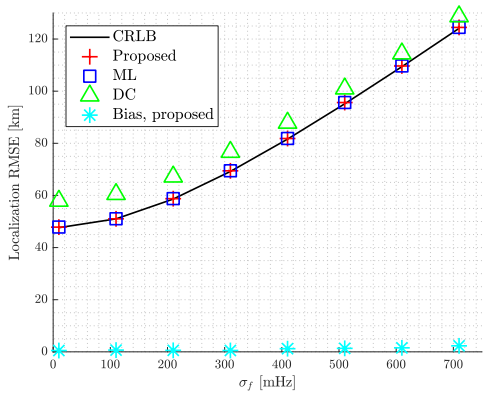

Fig. 3. Geolocation RMSE as a function of the FDOA noise standard deviation σ_f.

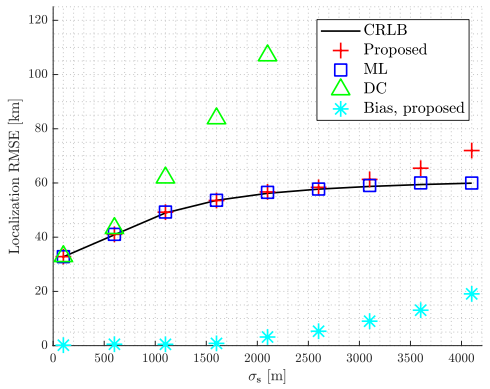

Fig. 4. Geolocation RMSE as a function of the satellite position error standard deviation σ_s.

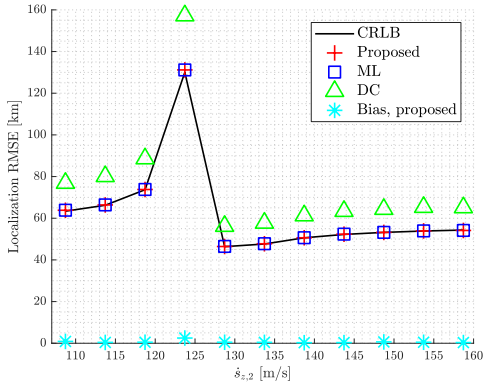

Fig. 5. Geolocation RMSE as a function of the z-axis velocity of satellite 2.

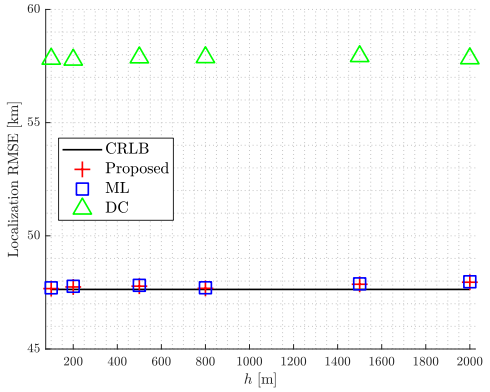

Fig. 6. Geolocation RMSE as a function of the assumed source altitude.

CPU and 12GB RAM. The DC-based technique, on the other hand, is unable to offer the CRLB performance under small TDOA noise, because it does not take into consideration the statistical information on the satellite location errors when performing measurement differencing. Note that as σ_t increases over 0.2μs, the performance of the DC-based approaches the CRLB. This is possibly because the TDOA noise now dominates the equivalent error covariance matrix $\hat{\mathbf{Q}}_y$ (see (29)) and the effect of the satellite location errors is less influential Notice that the estimation bias of the proposed algorithm is always less than 3km, which is negligible compared with the geolocation RMSE. It indicates that the proposed algorithm is approximately unbiased in this simulation.

Fig. 3 shows the results as a function of the FDOA noise standard deviation σ_f. The obtained observations are similar to those from Fig. 2. Again, as expected, the proposed two-step algorithm attains the CRLB accuracy.

Fig. 4 compares the geolocation performance as a function of the satellite position error standard deviation $\sigma_{\mathbf{s}}$. When $\sigma_{\mathbf{s}}$ is smaller than 2500m, the geolocation RMSEs of both the proposed two-step method and ML estimator remain very close to the CRLB. However, the performance of the proposed algorithm starts to deviate from the CRLB and become inferior to that of the ML estimator, as the satellite position error further increases. This is because the proposed algorithm does not refine the noisy satellite locations, in contrast to the ML estimator that estimates all the unknowns simultaneously.This is also the reason why the bias of the proposed algorithm increases apparently when $\sigma_{\mathbf{s}}$ is larger than 2500m. The geolocation performance of the DC-based method is very sensitive to the satellite position error and it degrades significantly as $\sigma_{\mathbf{s}}$ has larger values. We also investigated the geolocation performance as a function of the satellite velocity error standard deviation $\sigma_{\dot{s}}$. The observations are very similar and hence, the obtained results are omitted here.

Inspired by [36], we consider in Fig. 5 the impact of different satellite velocity configurations on the geolocation performance of the three algorithms simulated. In particular, the velocity of satellite 2 is *artificially* varied using $\dot{\mathbf{s}}_2^o + k \cdot [0, 0, 5]^T$. It can be seen that the geolocation performance changes greatly under different satellite velocity configurations, mainly because they affect the amount of information provided by the FDOA measurements on the source position (see (3)).

Fig. 6 shows the geolocation performance as a function of the assumed source altitude. Specifically, the true source altitude is unknown (which is 100m) and practically some

certain values of h are adopted in geolocation instead. As shown, the proposed algorithm and ML algorithm remain very close to the CRLB, while the DC-based produces obviously larger location errors. In a whole, the proposed algorithm, as well as the other two approaches, is insensitive to the error in the source altitude.

VI. Conclusions

We investigated the problem of dual-satellite source geolocation when time and frequency offsets between satellites and satellite location errors are present. The source position CRLB was derived. The insights from the CRLB analysis motivated the development of a closed-form two-step geolocation algorithm. In its Step-1 processing, the new method fuses using a BLUE the TDOAs and FDOAs from the source and calibration stations to produce as the output a single pair of source TDOA and FDOA. The time and frequency offsets are eliminated and the satellite location errors are taken into account in the weighting matrix of the BLUE. The second step of the proposed algorithm geolocates the source using the Step-1 output and the noisy satellite locations using an existing algebraic solution. Simulations using a short-baseline dual-satellite geolocation scenario verified the theoretical performance analysis result that the proposed algorithm can attain the CRLB performance under Gaussian noise and mild conditions.

In the future work, we plan to verify the proposed algorithm with practical satellites data. Furthermore, we plan to extend the proposed geolocation framework to the more general case with multiple satellites and satellite location refinement for further performance enhancement.

Appendix

Expressions for the partial derivatives $\left(\frac{\partial \mathbf{u}^o}{\partial \boldsymbol{\theta}^o}\right)$, $\left(\frac{\partial \mathbf{d}_u^o}{\partial \boldsymbol{\theta}^o}\right)$ and $\left(\frac{\partial \mathbf{y}^o}{\partial \boldsymbol{\beta}^o}\right)$ are provided here to complete the derivation of the source geolocation CRLB in (22).

From the definition $\boldsymbol{\theta}^o = [\phi, \varphi]^T$, the partial derivative $\left(\frac{\partial \mathbf{u}^o}{\partial \boldsymbol{\theta}^o}\right)$ can be easily shown to be equal to

$$\left(\frac{\partial \mathbf{u}^o}{\partial \boldsymbol{\theta}^o}\right) = \left[\left(\frac{\partial \mathbf{u}^o}{\partial \phi}\right), \left(\frac{\partial \mathbf{u}^o}{\partial \varphi}\right)\right]. \tag{37}$$

The detailed expression can be easily found using (1) and will be omitted here.

In the following derivation, we need the following definitions. Specifically, $\boldsymbol{\rho}_{\mathbf{a},\mathbf{b}} = \frac{(\mathbf{a}-\mathbf{b})}{||\mathbf{a}-\mathbf{b}||}$ denotes a unit vector from $\mathbf{b}$ to $\mathbf{a}$ and $\mathbf{g}_{\mathbf{a},\mathbf{b}} = -\frac{\dot{\mathbf{b}}}{||\mathbf{a}-\mathbf{b}||} + \frac{(\mathbf{a}-\mathbf{b})^T\dot{\mathbf{b}}}{||\mathbf{a}-\mathbf{b}||^2}\boldsymbol{\rho}_{\mathbf{a},\mathbf{b}}$.

By Chain Rule, $\left(\frac{\partial \mathbf{d}_u^o}{\partial \boldsymbol{\theta}^o}\right)$ can be expressed as

$$\left(\frac{\partial \mathbf{d}_u^o}{\partial \boldsymbol{\theta}^o}\right) = \left(\frac{\partial \mathbf{d}_u^o}{\partial \mathbf{u}^o}\right)\left(\frac{\partial \mathbf{u}^o}{\partial \boldsymbol{\theta}^o}\right) \tag{38}$$

where $\left(\frac{\partial \mathbf{u}^o}{\partial \boldsymbol{\theta}^o}\right)$ is given in (37) and $\left(\frac{\partial \mathbf{d}_u^o}{\partial \mathbf{u}^o}\right)$ is equal to, from (3),

$$\left(\frac{\partial \mathbf{d}_u^o}{\partial \mathbf{u}^o}\right) = \begin{bmatrix}\boldsymbol{\rho}_{\mathbf{u}^o,\mathbf{s}_1^o}^T - \boldsymbol{\rho}_{\mathbf{u}^o,\mathbf{s}_2^o}^T \\ \mathbf{g}_{\mathbf{u}^o,\mathbf{s}_1^o}^T - \mathbf{g}_{\mathbf{u}^o,\mathbf{s}_2^o}^T\end{bmatrix}. \tag{39}$$

Using (8), we have that

$$\left(\frac{\partial \mathbf{y}^o}{\partial \boldsymbol{\beta}^o}\right) = \left[\left(\frac{\partial \mathbf{d}_u^o}{\partial \boldsymbol{\beta}^o}\right)^T, \left(\frac{\partial \mathbf{d}_{c,1}^o}{\partial \boldsymbol{\beta}^o}\right)^T, ..., \left(\frac{\partial \mathbf{d}_{c,N}^o}{\partial \boldsymbol{\beta}^o}\right)^T\right]^T. \tag{40}$$

From (3) and (7), it can be shown that

$$\left(\frac{\partial \mathbf{d}_u^o}{\partial \boldsymbol{\beta}^o}\right) = \begin{bmatrix}-\boldsymbol{\rho}_{\mathbf{u}^o,\mathbf{s}_1^o}^T & \mathbf{0}^T & \boldsymbol{\rho}_{\mathbf{u}^o,\mathbf{s}_2^o}^T & \mathbf{0}^T \\ -\mathbf{g}_{\mathbf{u}^o,\mathbf{s}_1^o}^T & -\boldsymbol{\rho}_{\mathbf{u}^o,\mathbf{s}_1^o}^T & \mathbf{g}_{\mathbf{u}^o,\mathbf{s}_2^o}^T & \boldsymbol{\rho}_{\mathbf{u}^o,\mathbf{s}_2^o}^T\end{bmatrix} \tag{41a}$$

$$\left(\frac{\partial \mathbf{d}_{c,n}^o}{\partial \boldsymbol{\beta}^o}\right) = \begin{bmatrix}-\boldsymbol{\rho}_{\mathbf{c}_n,\mathbf{s}_1^o}^T & \mathbf{0}^T & \boldsymbol{\rho}_{\mathbf{c}_n,\mathbf{s}_2^o}^T & \mathbf{0}^T \\ -\mathbf{g}_{\mathbf{c}_n,\mathbf{s}_1^o}^T & -\boldsymbol{\rho}_{\mathbf{c}_n,\mathbf{s}_1^o}^T & \mathbf{g}_{\mathbf{c}_n,\mathbf{s}_2^o}^T & \boldsymbol{\rho}_{\mathbf{c}_n,\mathbf{s}_2^o}^T\end{bmatrix} \tag{41b}$$

where $n = 1, 2, ..., N$. This completes the derivation of the partial derivatives required in the CRLB result in Section III.

References

[1] K. Radnosrati, F. Gunnarsson, and F. Gustafsson, "New trends in radio network positioning," in *Proc. International Conference on Information Fusion (FUSION)*, 2015, pp. 492–498.

[2] K. Radnosrati, C. Fritsche, G. Hendeby, F. Gunnarsson, and F. Gustafsson, "Fusion of TOF and TDOA for 3GPP positioning," in *Proc. International Conference on Information Fusion (FUSION)*, 2016.

[3] K. C. Ho and Y. T. Chan, "Geolocation of a known altitude object from TDOA and FDOA measurements," *IEEE Transactions on Aerospace and Electronic Systems*, vol. 33, pp. 770–783, July 1997.

[4] M. Sun and K. C. Ho, "Refining inaccurate sensor positions using target at unknown location," *Signal Processing*, vol. 92, pp. 2097–2104, Sep. 2012.

[5] J. Geeraert, J. W. McMahon, and B. A. Jones, "Orbit determination observability of the dual-satellite geolocation system with TDOA and FDOA," in *Proc. AIAA/AAS Astrodynamics Specialist Conference*, 2016, pp. 5367–5388.

[6] D. P. Haworth, N. G. Smith, R. Bardelli, and T. Clement, "Interference localization for EUTELSAT satellites-the first European transmitter location system," *International Journal of Satellite Communications and Networking*, vol. 15, pp. 155–183, July 1997.

[7] M. H. Chan, "Application of a dual satellite geolocation system on locating sweeping interference," *World Academy of Science, Engineering and Technology*, vol. 6, pp. 939–944, September 2012.

[8] F. Guo, Y. Fan, Y. Zhou, C. Zhou, and Q. Li, *Space Electronic Reconnaissance: Localization Theories and Methods*. Hoboken, NJ, USA: Wiley, 2014.

[9] S. Stein, "Algorithms for ambiguity function processing," *IEEE Transactions on Acoustics, Speech, and Signal Processing*, vol. 29, pp. 588–599, June 1981.

[10] C. L. Yatrakis, "Computing the cross ambiguity function - a review," Master's thesis, Binghamton University, State University of New York, 2005.

[11] J. Overfield, Z. Biskaduros, and R. M. Buehrer, "Geolocation of MIMO signals using cross ambiguity function and TDOA/FDOA," in *Proc. IEEE International Conference on Communications (ICC)*, 2012, pp. 3648–3653.

[12] D. Roddi, *Satellite Communications*, 4th ed. New York, USA: McGraw Hill, 2006.

[13] M. Sun and L. Yang, "On the joint time synchronization and source localization using TOA measurements," *International Journal of Distributed Sensor Networks*, vol. 2013, Feb. 2013.

[14] Y. Cao, P. Li, J. Li, L. Yang, and F. Guo, "A new iterative algorithm for geolocating a known altitude target using TDOA and FDOA measurements in the presence of satellite location uncertainty," *Chinese Journal of Aeronautics*, vol. 28, pp. 1510–1518, September 2015.

[15] T. Pattison and S. I. Chou, "Sensitivity analysis of dual-satellite geolocation," *IEEE Transactions on Aerospace and Electronic Systems*, vol. 36, pp. 56–71, January 2000.

[16] H. Yan, J. K. Cao, and L. Chen, "Study on location accuracy of dual-satellite geolocation system," in *Proc. IEEE International Conference on Signal Processing (ICSP)*, 2010, pp. 107–110.

[17] K. C. Ho and L. Yang, "On the use of a calibration emitter for source localization in the presence of sensor position uncertainty," *IEEE Transactions on Signal Processing*, vol. 56, pp. 5758–5772, December 2008.

[18] L. Yang and K. C. Ho, "Alleviating sensor position error in source localization using calibration emitters at inaccurate locations," *IEEE Transactions on Signal Processing*, vol. 58, pp. 67–83, January 2010.

[19] J. Li, F. Guo, L. Yang, and W. Jiang, "On the use of calibration sensors in source localization using TDOA and FDOA measurements," *Digital Signal Processing*, vol. 27, pp. 33–43, April 2014.

[20] S. M. Kay, *Fundamentals of Statistical Signal Processing, Estimation Theory*. Upper Saddle River, NJ, USA: Prentice Hall, 1993.

[21] A. Yeredor, "On passive TDOA and FDOA localization using two sensors with no time or frequency synchronization," in *Proc. IEEE International Conference on Acoustics, Speech, and Signal Processing (ICASSP)*, 2013, pp. 4066–4070.

[22] O. Jean and A. J. Weiss, "Convex joint emitter localization and passive sensor network synchronization," in *Proc. IEEE Workshop on Sensor Array and Multichannel Signal Processing (SAM)*, 2012, pp. 201–204.

[23] S. Zhou and Z. Ding, "Joint synchronization and localization using TOAs: a linearization-based WLS solution," *IEEE Journal on Selected Areas in Communications*, vol. 28, pp. 1016–1025, September 2010.

[24] Y. Wang, J. Huang, L. Yang, and Y. Xue, "TOA-based joint synchronization and source localization with random errors in sensor positions and sensor clock biases," *Ad Hoc Networks*, vol. 27, pp. 99–111, April 2015.

[25] J. Liu, Z. Wang, J. Cui, S. Zhou, and B. Yang, "A joint time synchronization and localization design for mobile underwater sensor networks," *IEEE Transactions on Mobile Computing*, vol. 15, pp. 530–543, March 2016.

[26] H. H. Fan and C. Yan, "Asynchronous differential TDOA for sensor self-localization," in *Proc. IEEE International Conference on Acoustics, Speech, and Signal Processing (ICASSP)*, 2007, pp. 1109–1112.

[27] C. Yan and H. H. Fan, "Asynchronous differential TDOA for non-GPS navigation using signals of opportunity," in *Proc. IEEE International Conference on Acoustics, Speech, and Signal Processing (ICASSP)*, 2008, pp. 5312–5315.

[28] Y. Wang, X. Ma, and G. Leus, "Robust time-based localization for asynchronous networks," *IEEE Transactions on Signal Processing*, vol. 59, pp. 4397–4410, Sep. 2011.

[29] Y. Wang and K. C. Ho, "TDOA source localization in the presence of synchronization clock bias and sensor position errors," *IEEE Transactions on Signal Processing*, vol. 61, September 2013.

[30] P. D. Groves, *Principles of GNSS, Inertial, and Multisensor Integrated Navigation Systems*, 2nd ed. Boston, MA, USA: Artech House, 2013.

[31] P. Stoica and B. C. Ng, "On the Cramer-Rao bound for parametric constraints," *IEEE Signal Processing Letters*, vol. 5, pp. 177–179, July 1998.

[32] T. J. Moor, R. J. Kozick, and B. M. Sadler, "The constrainted Cramer-Rao bound from the perspective of fitting a model," *IEEE Signal Processing Letters*, vol. 14, pp. 564–567, August 2007.

[33] Y. Hu and G. Leus, "On a unified framework for linear nuisance parameters," *EURASIP Journal on Advances in Signal Processing*, vol. 2017, 2017.

[34] C.-I. Chang, "Orthogonal subspace projection (OSP) revisited: a comprehensive study and analysis," *IEEE Transactions on Geoscience and Remote Sensing*, vol. 43, pp. 502–518, March 2005.

[35] M. Song and C.-I. Chang, "A theory of recursive orthogonal subspace projection for hyperspectral imaging," *IEEE Transactions on Geoscience and Remote Sensing*, vol. 53, pp. 3055–3072, June 2015.

[36] H. Hmam, "Optimal sensor velocity configuration for tdoa-fdoa geolocation," *IEEE Transactions on Signal Processing*, vol. 65, pp. 628–637, February 2017.